Chapter 1

INTRODUCTION

Focusing and imaging correspond to two basic requirements in utilizing light: manipulating and observing. Optical focusing and imaging are of great importance in biomedicine, remote sensing, astronomy, industrial production, to name a few. The advantage of using light can be summarized in three aspects, as follows.

First, optical resolution is only limited by diffraction, and can reach sub-micrometer scale [1]. It enables optical focusing to have a precise spatial selectivity, which allows for stimulation or manipulation of micro structures and micro processes. For example, photolithography [2, 3] is an indispensable tool for integrated circuit fabrication, and optical focusing is also widely used for the control of cellular or subcellular biological systems, such as in photodynamic therapy [4], photoreleasing [5], optogenetics [6, 7], and optical cell trapping and shearing [8, 9]. Optical imaging with its fine resolution opens a door to the microworld through direct visualization. Optical microscopy [10, 11] has long been a reliable tool in diagnosis. Recent development in super-resolution microscopy [12–16] has pushed the resolution limit down to tens of nanometers, even several nanometers. Although electron [17] and scanning probe microscopy [18, 19] inherently possess a finer resolution (subnanometer), optical microscopy is still the only way to observe living processes at micro scale without harsh preparation procedures.

Second, due to the physical interaction between light and matter, it is possible to use optical focusing and imaging to investigate material compositions through spectroscopy, polarization, photoluminescence, and photoacoustics [20]. For instance, Raman spectroscopy [21–24] is extensively used to observe vibrational, rotational, and other low-frequency modes in a molecular system.

Third, optical focusing and imaging have the ability to perform at high temporal resolution. It enables us to control and observe temporal evolution of physical events, which led to the advent of ultrafast optics [25]. Tremendous efforts have been made in the development of ultrafast spectroscopy [26, 27], laser-controlled chemistry, and so on, among which one exciting achievement is that the world's fastest 2-D camera up to date can capture events at up to 100 billion frames per second [28].

Conventionally, optical focusing and imaging are realized by lenses in a transparent medium, like air or glass, which are based on the ballistic propagation of light. However, when light propagates through most scattering media, refractive index inhomogeneities cause diffuse scattering that increases with depth. This poses a major challenge to all the aforementioned optical methods. Moreover, glare caused by backscattering will largely impair the visibility of imaging, and time-varying scattering by dynamic media will also pose a challenge to the system response time. All of these factors fundamentally limit the feasibility of optical focusing and imaging in scattering media, such as biological tissues and fog. In this chapter, we provide an overview of the physics behind optical scattering, discuss the challenges brought in, and introduce different methods used to overcome scattering.

1.1 Physics of Scattering

Light interacts with matter in many different ways including absorption, elastic scattering, inelastic scattering, quasi-elastic scattering, nonlinear process. Here we limit our discussion to elastic scattering, which causes light to diffusively propagate in scattering media. We will first start with single particle scattering model, and then expand our discussion to a group of particles. Finally, based on the model, we will discuss the properties of real scattering media and conclude with some general "rules of thumb" that are useful when considering the interaction of light with tissue.

Scattering of a single particle

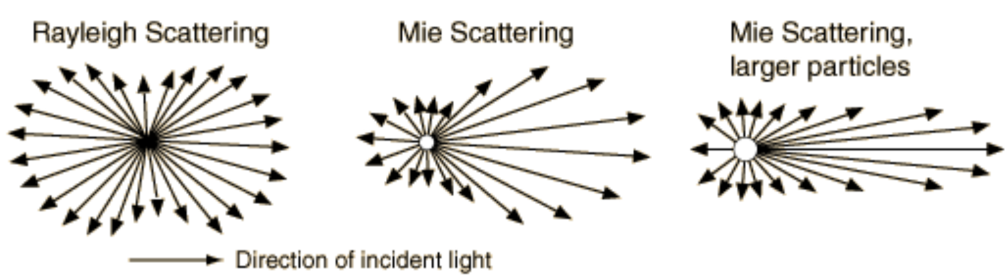

Figure 1.1: Rayleigh scattering and Mie scattering [29]

A simple model to start with is the scattering of a single small particle, which can be described as Rayleigh scattering or Mie scattering [30–32], as shown in Fig. 1.1. For particles much smaller than the wavelength of the incident light, their scattering of light can be explained by Rayleigh scattering. It is an approximation derived from the interaction between light and a dipole. The scattered intensity distribution $I(r, \theta)$

(expressed in polar coordinates) for unpolarized incident light can be expressed as [30, 32]

$$I_s(r,\theta) = 8\pi^4 {n_{su}}^4 (\frac{{n_s}^2 - {n_{su}}^2}{{n_s}^2 + 2{n_{su}}^2}) \frac{a^6}{r^2\lambda^4}(1+\cos^2\theta) I_0, \tag{1.1.1}$$

where I_0 is the incident light intensity, λ is its wavelength, n_s and n_{su} are the respective refractive indices of the scatterer and its surrounding medium, and a is the radius of the scatterer.

Mie scattering is applied when the particle size is on the order of the wavelength. It can be derived by solving Maxwell's equations for the case of a spherical scatter, composed of homogeneous and isotropic material, that is irradiated by a monochromatic plane wave [33]. The angular intensity distribution of scattered light for two perpendicular polarizations can be describe as,

$$I_1(\theta) = \left| \sum_{n=1}^{\infty} \frac{2n+1}{n(n+1)} [a_n \pi_n(\cos\theta) + b_n \tau_n(\cos\theta)] \right|^2, \tag{1.1.2}$$

$$I_2(\theta) = \left| \sum_{n=1}^{\infty} \frac{2n+1}{n(n+1)} [b_n \pi_n(\cos\theta) + a_n \tau_n(\cos\theta)] \right|^2, \tag{1.1.3}$$

where a_n and b_n are coefficients defined by the boundary conditions, and $\pi_n(\cos\theta)$ and $\tau_n(\cos\theta)$ are the Mie angular functions. The functions can be described as

$$\pi_n(\cos\theta) = \frac{1}{\sin\theta} P_n^1(\cos\theta), \tag{1.1.4}$$

$$\tau_n(\cos\theta) = \frac{d}{d\theta} P_n^1(\cos\theta), \tag{1.1.5}$$

where P_n^1 are associated Legendre polynomials of the first kind. In both cases, we can conclude that incident beam is deflected from its original propagation. A narrow incident beam will be scattered into a cone of beams with different directions. Aside from forward scattering, there is backscattering as well.

Based on the single particle model, we can derive more parameters to characterize the scattering of light by a single particle. One important parameter is the scattering anisotropy g [32],

$$g =< \cos(\theta) > , \tag{1.1.6}$$

where θ is the scattering angle. g describes the angular spread of light scattered off a particle. The values of g can range from -1 to 1, where a lower negative value indicates more backward scattering, while a higher positive value indicates more forward scattering. Another important parameter for a single scatterer is its scattering cross section σ_s [mm^2]. σ_s indicates the particle's scattering capability. It can be thought of as the effective area that guarantees scattering when a photon impinges. σ_s is related to its geometric cross-sectional area A [mm^2] by the proportionality constant called the scattering efficiency Q_s [dimensionless], which is described as $\sigma_s = Q_s A$. Note that Q_s takes on a statistical nature and is not necessarily equal to the physical cross section area of the scatterer.

Scattering of a collection of particles

Based on the scattering model of a single scatterer, we expand our discussion to the scattering of a collection of homogeneous scatterers that are randomly distributed within a finite three-dimensional space. This is a simplified model of a real scattering medium. The scattering characteristics of the sample per unit length are described by the scattering coefficient μ_s [mm^{-1}] and the scattering mean free path (MFP) l_s [mm]:

$$\mu_s = \sigma_s N, \tag{1.1.7}$$

$$l_s = \frac{1}{\mu_s}, \tag{1.1.8}$$

where N is the number of scatterers per unit volume [mm^{-3}]. The scattering MFP is the average distance between scattering events. From l_s, we can derive the intensity of ballistic light after light travels a thickness of l through the sample [32],

$$I_b(l) = I_0 e^{-\frac{l}{l_s}} = I_0 e^{-\mu_s l}. \tag{1.1.9}$$

Eq. 1.1.9 only quantifies how many photons are scattered. It doesn't consider how much the photons have deviated from their original trajectory. For example, if $g \approx 1$ and a photon encounters many scattering events, the trajectory of the photon will still not deviate from its ballistic trajectory too much. In other words, the photon retains some "memory" of its original orientation. To eliminate this "memory", the anisotropy of the scatterers is incorporated to characterize the scattering sample by their reduced scattering coefficient $\mu_s{}'$ [mm^{-1}] or transport mean free path (TMFP) $l_s{}'$ [mm], which are defined as,

$$\mu_s{}' = (1 - g)\mu_s, \tag{1.1.10}$$

$$l_s{}' = \frac{1}{\mu_s{}'}. \tag{1.1.11}$$

From the equations, we can tell $\mu_s{}'$ is a lumped property incorporating μ_s and g. By multiplying μ_s by a factor of $(1 - g)$, we convert the photon movement with many small steps $1/\mu_s$ that involve only partial deflection to a random walk of step size $1/\mu_s'$. We can think of the TMFP as the mean distance after which a photon's direction becomes randomized. By the definition of MFP and TMFP, people divide light propagation in scattering media into four different regimes [32, 34, 35]. Within one MFP through a scattering media, ballistic photons are still dominant. This regime is called ballistic regime. In the region from the MFP to the TMFP, photons are scattered a few times but are just slightly deflected from their paths. This regime is called the quasi-ballistic regime. Between one and ten TMFPs, incident photons have been scattered many times but still retain some "memory" of their original directionality. This regime is called quasi-diffusive regime. Finally, beyond ten TMFPs, the directions of the scattered photons are barely related to its original directions. This regime is called diffusive regime. If you want to directly visualize the difference of scattering in different regimes, please refer to a schematic depiction from Vasilis Ntziachristos's paper [34].

The particle model described above is an inaccurate approximation for a real scattering medium. Consider the case of biological tissue for example. Its micro-structure is more complicated than smaller particles of the same identity suspended in a uniform environment. Biological tissues can have micro structures ranging from 0.01 μm for membranes to 10 μm for whole cells [32, 36]. The refractive indices of scatterers can also vary from 1.34-1.62 for different tissue components [32, 36]. Therefore, it is really difficult to solve the scattering of a real scattering medium through all the micro processes and then find a solution to counter its influence. However, the model we use is accurate enough when considering the scattering process at the macro scale, such as in estimating the portion of ballistic transmission and randomness of transmitted wavefront. We may have a chance to draw some useful conclusions from the macro-phenomena of scattering and then come to some useful tools by either resolving or utilizing scattering. This leads to the discussions in the following sections.

1.2 Macro-Phenomena of Scattering

Speckle

When a single optical mode is shone onto a scattering medium, light propagates diffusively within the scattering medium, as shown in Fig.1.2(a). The concept of optical mode will be discussed in the end of this section. For now, we can just take it as a beam that is perfectly monochromatic and as narrow as possible. After traveling beyond the diffusive regime, the output will be a spatially uncorrelated

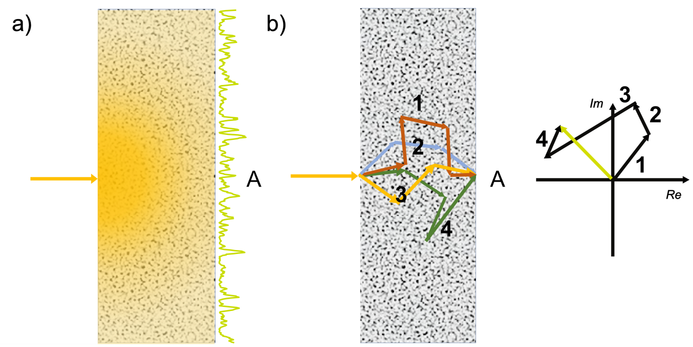

Figure 1.2: Schematic depiction of light's diffusive propagation and output wavefront through a scattering medium. (a) A perfectly monochromatic beam propagates through a scattering medium. (b) At an arbitrary point on the output wavefront, the electric field can be deemed as a summation of different beamlets.

wavefront. Initially, we limit attention to a single polarization state, since the same analysis will apply for the other polarization. At an arbitrary point A(x,y) on the output surface $z = z_{output}$, the output optical field is a summation of beamlets that encounter different scattering events, as shown in Fig. 1.2(b). Moreover, from the previous section we know that the scattering of each beamlet can be considered a random process. Thus, we can consider the output electric field of every beamlet at point A as a random variable $a_k(x, y)$ and the output electric field at point A, $E(x, y)$ can be described as summation of $a_k(x, y)$ in the complex plane as shown in Fig. 1.2(b),

$$E(x, y) = \sum_{k=1}^{N} a_k(x, y) = \sum_{k=1}^{N} |a_k(x, y)| e^{i\theta_k}, \tag{1.2.1}$$

where $|a_k(x, y)|$ and θ_k are the amplitude and phase of a_k, respectively. If we decompose $E(x, y)$ into the real and imaginary parts, we have

$$E(x, y) = \mathrm{Re}(E(x, y)) + i\,\mathrm{Im}(E(x, y)), \tag{1.2.2}$$

$$\mathrm{Re}(E(x, y)) = \sum_{k=1}^{N} |a_k(x, y)| \cos\theta_k, \tag{1.2.3}$$

$$\mathrm{Im}(E(x, y)) = \sum_{k=1}^{N} |a_k(x, y)| \sin\theta_k. \tag{1.2.4}$$

We know that $a_k(x, y)$ is generated by the incident beam with limited energy, so $|a_k(x, y)|$ should possess limited mean value and variance. Note that we have only shown four $a_k(x, y)$s that sum up at point A in Fig. 1.2(b). In fact, N is very large, considering the fact of diffusive propagation of light in the medium. Therefore, we can apply the central limit theorem to Eqs.1.2.3 and 1.2.4, which simply means $\mathrm{Re}(E(x, y, z))$ and $\mathrm{Im}(E(x, y))$ follow a Gaussian distribution. By evaluating their first-order statistical properties, we can find out that the real and imaginary parts of the output field have zeros means, identical variances, and are uncorrelated. Supposing $\mathrm{Re}(E(x, y))$ follows a Gaussian distribution with zero mean and variance σ^2, the joint probability function of $\mathrm{Re}(E(x, y))$ and $\mathrm{Im}(E(x, y))$ is

$$p(\mathrm{Re}(E(x, y)), \mathrm{Im}(E(x, y))) = \frac{1}{2\pi\sigma^2} \exp\left(-\frac{[\mathrm{Re}(E(x, y))]^2 + [\mathrm{Im}(E(x, y))]^2}{2\sigma^2}\right). \tag{1.2.5}$$

Such a density function is commonly known as a circular Gaussian density function. Therefore, $E(x, y)$ can be referred to as a circular complex Gaussian random variable.

For the output wavefront, it is more straightforward to talk about its amplitude $|E(x, y)|$, intensity $I(x, y)$, and phase $\theta(x, y)$. We can apply the transformation of these random variables with reference to $\mathrm{Re}(E(x, y))$ and $\mathrm{Im}(E(x, y))$ as follows:

$$|E(x, y)| = \sqrt{[\mathrm{Re}(E(x, y)]^2 + [\mathrm{Im}(E(x, y)]^2}, \tag{1.2.6}$$

$$I(x, y) = [\mathrm{Re}(E(x, y)]^2 + [\mathrm{Im}(E(x, y)]^2, \tag{1.2.7}$$

$$\theta = Arg(\mathrm{Re}(E(x, y)) + i\,\mathrm{Im}(E(x, y))). \tag{1.2.8}$$

Then the probability density functions of $|E(x, y)|$, $I(x, y)$ and $\theta(x, y)$ are

$$p(|E(x, y)|) = \begin{cases} \frac{1}{\sigma^2} \exp\left(\frac{-|E(x,y)|^2}{2\sigma^2}\right) & ,\text{if } |E(x, y)| \geq 0 \\ 0 & ,\text{otherwise} \end{cases}, \tag{1.2.9}$$

$$p(I(x, y)) = \begin{cases} \frac{1}{2\sigma^2} \exp\left(\frac{-I(x,y)}{2\sigma^2}\right) & ,\text{if } |I(x, y)| \geq 0 \\ 0 & ,\text{otherwise} \end{cases}, \tag{1.2.10}$$

$$\text{and } p(\theta(x, y)) = \begin{cases} \frac{1}{2\pi} & ,\text{if } -\pi \leq \theta(x, y) < \pi \\ 0 & ,\text{otherwise} \end{cases}. \tag{1.2.11}$$

From the equations, we can conclude that the intensity of the output wavefront follows a negative exponential distribution, the amplitude follows a Rayleigh distribution, and the phase possesses a uniform distribution [37]. The phase and amplitude are independent. The statistics have been confirmed in experiment. Fig. 1.3(a) is an intensity pattern of a scattered wavefront we captured by a CCD sensor with an objective lens. We can tell the two-dimensional intensity distribution is a speckle pattern. A two-dimensional histogram of the amplitude and phase of speckle pattern is shown in Fig. 1.3(b), which matches the probability distribution of phase and amplitude. Note that speckle is the smallest feature in a speckle pattern. The speckle size is defined by the diffraction limit $\frac{\lambda}{NA}$, where the numerical aperture NA is the sine of the maximum take-off angle of light on the output surface. By the Shannon's sampling theorem, within the half width of a speckle $\frac{\lambda}{2NA}$, the amplitude and phase can be deemed as uniform. An area of $(\frac{\lambda}{2NA})^2$ on the output surface can be treated as a single optical mode. This clarifies the definition of an optical mode at the beginning of this section. This is also why we can discretize a continuous wavefront into an array of discrete optical modes, which we will frequently use in the transmission matrix theory. A rigorous proof of wavefront discretization can be found in the supplementary material of reference [38].

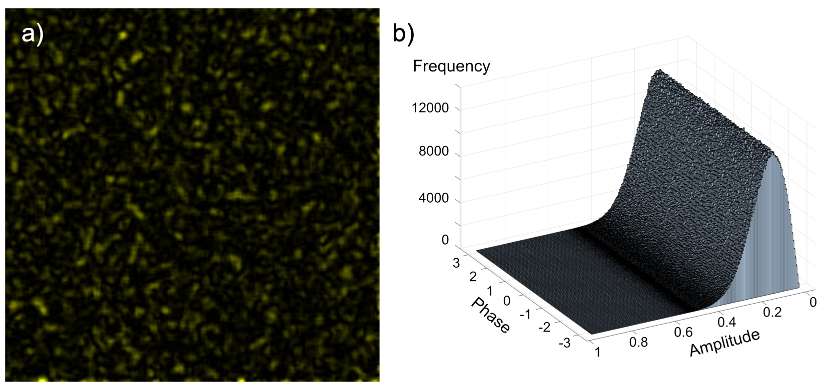

Figure 1.3: Statistics of the output scattering wavefront. (a) The spatial intensity pattern of the output scattering wavefront. (b) 2D histogram of the phase and amplitude of the output scattering wavefront.

The previous discussion was based on a single mode input. If we have a wide incident beam or multiple input modes, the conclusions still hold. Without loss of generality, let's suppose we have two input modes, their output wavefronts are $E_1(x, y)$ and $E_2(x, y)$. $\mathrm{Re}(E_1(x, y))$ and $\mathrm{Im}(E_1(x, y))$ follow a Gaussian distribution with zero mean and variance ${\sigma_1}^2$, while $\mathrm{Re}(E_2(x, y))$ and $\mathrm{Im}(E_2(x, y))$ follow a Gaussian distribution with zero mean and variance ${\sigma_2}^2$. If the incident beams are perfectly monochromatic, the output wavefront will be a coherent summation of $E_1(x, y)$ and $E_2(x, y)$. That is $E_{output}(x, y) = E_1(x, y) + E_2(x, y)$. If $E_1(x, y)$ and $E_2(x, y)$ are independent, $\mathrm{Re}(E_{output}(x, y))$ follows a Gaussian distribution with zero mean and variance ${\sigma_1}^2 + {\sigma_2}^2$ by calculating the probability density function of summation of independent random variables, as does $\mathrm{Im}(E_{output}(x, y))$. Going through the same derivation as the case of a single incident mode, we come to the same statistical properties for output wavefront from multiple input modes.

Transmission matrix theory

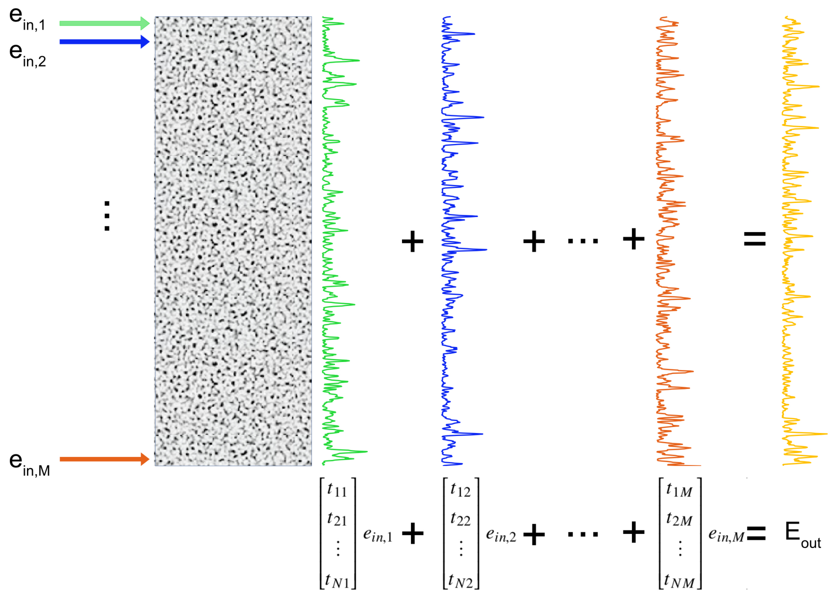

Figure 1.4: The output of a incident input wavefront can be deemed as the summation of the output wavefronts of every single input mode, as discussed in the previous section. The conclusion can also be expressed by the transmission matrix theorem as shown in Eq. 1.2.14.

If we treat the process through which light propagates inside the scattering media as a linear lossless process of the optical field and look at the input and output wavefronts, we can describe scattering as a linear transform between the two [39–41]. Based on the discussion in the speckle section, the input and output wavefronts can be discretized as elementwise arrays of optical modes. Suppose array E_{in} and array E_{out} represent the input and output wavefront and have M and N elements, respectively. Every element of E_{in} and E_{out} is the complex value of the corresponding optical mode. The transform can be represented by a N by M transmission matrix $T_{in\to out}$, which describes how the phase and amplitude of the input field is modified by the medium and presented on the output plane. Its mathematical representation is [40]

$$E_{out} = T_{in\to out} E_{in}. \tag{1.2.12}$$

To be more clear, an elementwise expression of Eq. 1.2.12 is

$$\begin{bmatrix} t_{11} & t_{12} & \dots & t_{1M} \\ t_{21} & t_{22} & \dots & t_{2M} \\ \vdots & \vdots & \ddots & \vdots \\ t_{N1} & t_{N2} & \dots & t_{NM} \end{bmatrix} \begin{bmatrix} e_{in,1} \\ e_{in,2} \\ \vdots \\ e_{in,M} \end{bmatrix} = \begin{bmatrix} t_{11}e_{in,1} + t_{12}e_{in,2} + \cdots + t_{1M}e_{in,M} \\ t_{21}e_{in,1} + t_{22}e_{in,2} + \cdots + t_{2M}e_{in,M} \\ \vdots \\ t_{N1}e_{in,1} + t_{N2}e_{in,2} + \cdots + t_{NM}e_{in,M} \end{bmatrix} = \begin{bmatrix} e_{out,1} \\ e_{out,2} \\ \vdots \\ e_{out,N} \end{bmatrix}, \tag{1.2.13}$$

where $e_{in,k}$ and $e_{out,k}$ are the kth element in array E_{in} and E_{out}, respectively and t_{ij} is the element at the ith row and jth column of the transmission matrix $T_{in\to out}$. If we take a close look at the terms on the left and right of the second equal sign in Eq. 1.2.13, we can rewrite the equation as

$$E_{out} = \left[\begin{bmatrix} t_{11} \\ t_{21} \\ \vdots \\ t_{N1} \end{bmatrix} e_{in,1} + \begin{bmatrix} t_{12} \\ t_{22} \\ \vdots \\ t_{N2} \end{bmatrix} e_{in,2} + \cdots + \begin{bmatrix} t_{1M} \\ t_{2M} \\ \vdots \\ t_{NM} \end{bmatrix} e_{in,M} \right], \tag{1.2.14}$$

which simply means that the output optical field is the summation of every individual output of a single input optical mode. A schematic demonstration is shown Fig. 1.4. In the previous section, we derived the statistics of the output wavefront of a single input mode. In transmission matrix theorem, for a defined input mode $e_{in,j}$, its output wavefront is described as an array $[t_{1j}e_{in,j}, t_{2p}e_{in,j}, \dots, t_{Nj}e_{in,j}]$. So that, $t_{k,j}e_{in,j}$ should follow the circular Gaussian distribution due to its statistical property. For a definite j, $e_{in,j}$ is a complex constant, so it is t_{ij} that possess a circular Gaussian distribution. In other words, every element in the same column of the transmission matrix follows a circular Gaussian distribution. If every column of the transmission matrix is independent, then every element t_{ij} in the transmission matrix $T_{in\to out}$ follows a circular Gaussian distribution. Generating a random matrix with circular Gaussian distributed elements is usually how people simulate a scattering medium. Transmission matrix theory is widely used in the analysis of wavefront shaping and phase conjugation. We will see more derivations based on this in the following sections.

Memory effect

In the previous section, we modeled the scattering as a transmission matrix. For a real scattering medium, its transmission matrix can have an additional macroscopic structure, either correlation in spatial domain or Fourier domain, depending on its scattering property. Memory effect is the manifestation of correlations in the

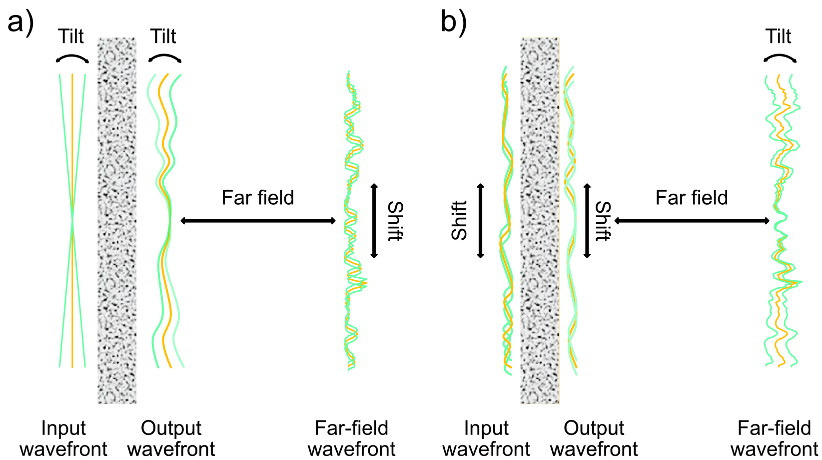

Figure 1.5: Schematic depiction of two types of memory effects. (a) Traditional memory effect. (b) Translational memory effect.

transmission matrix. Up to date, two types of memory effects have been discovered. They are the traditional memory effect [42, 43] and the translational memory effect [38], respectively.

The traditional memory effect for a general scalar wave was first derived theoretically in 1988 [42]. It was verified experimentally for optical waves in the same year [43]. The traditional memory effect describes the following phenomenon: when an input wavefront reaching a diffusing sample is titled within a certain angular range, the output wavefront is equally tilted, resulting in a spatial shift of the speckle pattern at far filed, as shown in Fig 1.5(a). The distance within which this property holds is called the memory effect region (MER). It can be approximated by the equation [38],

$$MER \approx \frac{v\lambda}{\pi L}, \tag{1.2.15}$$

where v is the distance from the output plane of the scattering medium to the screen, λ is the wavelength of the light source and L is the thickness of the scattering medium. From the equation, the MER is inversely proportional to the thickness of the scattering media. For useful applications, it requires the scattering medium to be thin. Moreover, it requires a distance of far-field propagation to realize the shift of the output wavefront. The conjugate planes of the tilt-and-shift relation is the input surface and the far-field plane. If we think inversely of the phenomenon, a point source within the MER will generate a random speckle pattern through the scattering medium. When we shift the point source, the speckle pattern will also shift at far field. If we treat the speckle pattern as a point spread function (PSF), the PSF will be shift-invariant within the MER, which is similar to the scenario in a traditional lens based imaging system. People have demonstrated direct image transfer and computational image recovery based on the traditional memory effect. We will see some related work we have done in Chapter 5.

The translational memory effect was first reported in 2015 [38]. It is a complementary type of memory effect to the traditional one. It describes the following phenomenon: when an input wavefront reaching an anisotropically scattering medium is shifted within a certain distance, the output wavefront is equally shifted, resulting in the tilting of far-filed wavefront, as shown in Fig. 1.5(b). The translational memory effect applies for thick and highly forward scattering media, such as biological samples. Different from the traditional memory effect, its shift-invariant PSF region is on the output surface the scattering medium, which has important implication for biomedical imaging and adaptive optics.

There are also many other macro-phenomena discovered on optical scattering, such as the shower-curtain effect [44–46] and Anderson localization [47–49]. We will not talk about them in detail.

1.3 The Problem of Scattering

As briefly discussed in the abstract, scattering is a major challenge for optical focusing and imaging. In this section, we will analyze three effects that hinder optical focusing and imaging through scattering media, which are wavefront aberrations, glare, and decorrelation.

Wavefront aberration

Wavefront aberrations originate from the diffusive propagation of forward-scattering light through scattering media. They are the differences between the scattered wavefront and the wavefront intended to present through a scattering medium. Wavefront aberrations induced by scattering are different from the wavefront aberration in a lens system [50, 51]. First, it cannot be predicted by the geometrical setup such as aperture size, propagation distance, and lens shape [52]. Second, the order of scattering wavefront aberration is very high, considering the fact that the output wavefront is made up of diffraction limited speckles. As such, the aberrations cannot be compensated by traditional lens design. As shown in Fig. 1.6(a), a collimated beam is focused on the focal plane by a lens in free space. However, if we applied the same strategy in the presence of a scattering medium, the outcome will be a speckle

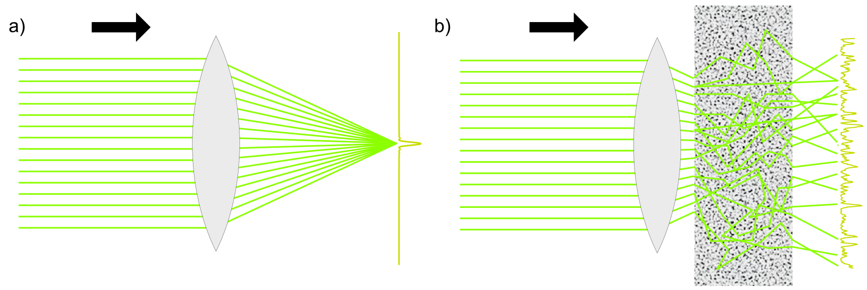

Figure 1.6: Schematic depiction of problem of scattering for focusing light through a scattering medium. (a) Optical focusing can be easily realized by a lens in free space. (b) Scattering media leads to a diffusive propagation, which results in a random output wavefront.

field on the focal plane. Based on the statistical property of speckle pattern, light intensity is not well confined to a small region so that it lost its spatial selectivity. For imaging, conventional imaging systems relies on lenses and mirrors to transform light from a point on the object plane to a point on the image plane [53, 54]. If there is a scattering medium in front of the object, the PSF will spread out as a speckle field. The point-to-point conjugate relationship between the object and image is broken by the wavefront aberrations. Therefore, conventional optical methods will fail when they are applied to imaging through scattering media.

Glare

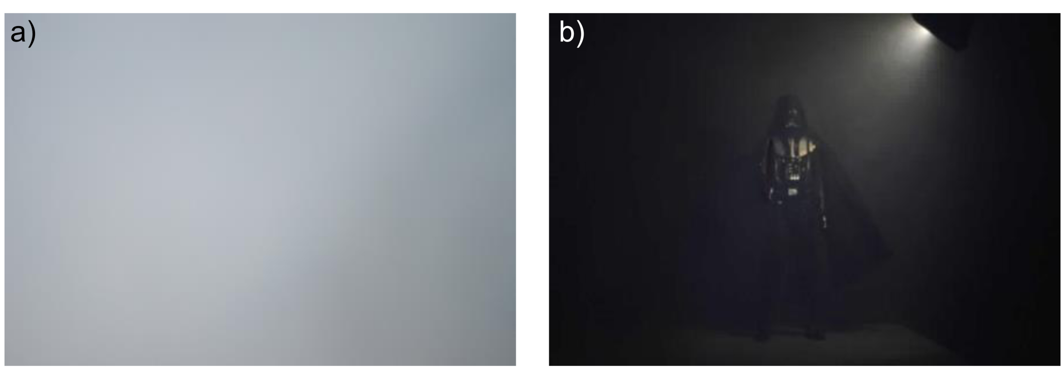

Figure 1.7: Experimental demonstration of issue brought by glare. (a) shows the captured camera image with a reflective illumination. The glare from the light source prevents us from seeing the target. (b) shows a captured image where the figurine is locally illuminated.

Glare is the undesired backward-scattering light when we illuminate a scattering sample [55, 56]. It impacts imaging more than focusing. When we try to image a target through a scattering medium, in most cases such as remote imaging in fog, haze, and sandstorm, we don't have access to the other side of the scattering media. Therefore, a reflective illumination setup has to be adopted over trans-illumination, which means the light source and the detector are on the same side with reference to the sample. In the reflective illumination scenario, light first propagates through the scattering medium before illuminating the target. The glare from the illumination source impinging on the scattering medium can mask the reflections from a weak distant target [57–59]. An experimental demonstration is shown in Fig. 1.7. This brief experiment illustrates the issue: glare can significantly reduce our ability to image or probe into scattering media. Here we point both a camera and a spotlight at a fog bank (generated by a fog machine). A figurine is on the other side of this fog bank. Fig. 1.7(a) shows the captured camera image with the spotlight illumination. The glare from the spotlight prevents us from seeing the figurine. Fig. 1.7(b) shows a captured image where the figurine is locally illuminated. Despite the slight blurring introduced by scattering from the fog, we can readily discern the figurine. The more challenging part is that the glare wavefront generated by a coherent light source is a speckle field with severe intensity variance. Even if an incoherent light source is used, the glare will still show up as an uneven noise term, as we can see from Fig. 1.7(a). Moreover, if the glare intensity is too high, its shot noise will overwhelm the signal. Glare as a strong background cannot be easily removed by simple digital signal processing such as background subtraction and contrast enhancement. Physical methods are required to suppress the glare or separate it from the target reflection.

Decorrelation

All the previous discussion is based on a static scattering media. However, many scattering media we frequently deal with are dynamic, whose micro structure or composition is changing over time. For example, living biological tissues can have blood cells moving continuously in the vessel. The refractive indices of cytoplasm in cells will also vary based on metabolism. Fog is made up of small droplets of water in the condensed phase. The water droplets are kept in the air by thermal Brownian motion. All of these micro changes will accumulate and lead to a time-varying output wavefront when we shine a coherent beam through the sample[60–63]. The change of the output wavefront can be described as a decorrelation process and characterized by its intensity autocorrelation function based on the diffusing-wave spectroscopy [64]. Suppose the mean intensities of speckle patterns at different times are the same, then the autocorrelation function can be written as [65, 66]

$$g_2(\tau) = \frac{< I(x,y,t_0)I(x,y,t_0+\tau) >_{x,y}}{< I(x,y) >_{x,y}{}^2} - 1, \tag{1.3.1}$$

where $< >_{x,y}$ represents the ensemble-average in the capture plane, $I(x, y, t)$ is the speckle pattern at time t, and τ is the time interval. According to the assumption, $< I(x, y) >_{x,y}=< I(x, y, t_0)_{x,y} >=< I(x, y, t_0 + \tau)_{x,y} >$. $g_2(\tau)$ is the correlation factor. From the statistics of speckle, we know that $g_2(\tau)$ can range from 0 to 1,

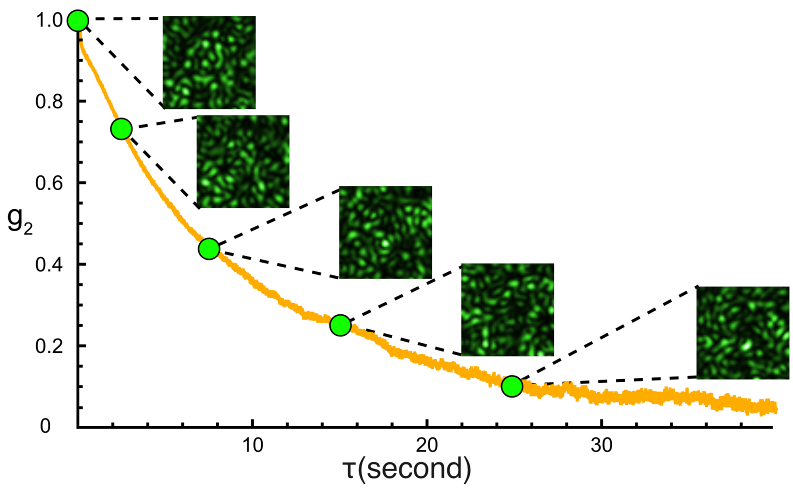

Figure 1.8: Measured decorrelation curve of a 1 mm thick rat brain tissue.

which corresponds the change of correlation. Then the speed of decorrelation can be describe as $\Delta g_2/\tau$. However, as shown in Fig. 1.8, the decorrelation process doesn't always follow a linear fashion. Fig.1.8 is an example of a decorrelation curve measured in experiment. Therefore, decorrelation time is more commonly used to describe how fast a tissue decorrelates. It is the time interval τ after which the $g_2(\tau)$ autocorrelation factor decays to a pre-determined value, typically $1/e^2$, $1/e$ [66–71]. If we choose $1/e^2$ as a standard, for example, the decorrelation time τ_{1/e^2} for the dorsal skin of a living mouse with 1.5 mm thickness can be shorter than 50 ms [66, 69].

Decorrelation poses a challenge for the techniques that work under the assumption that scattering is static. For example, wavefront shaping technique is a novel technique that can focus light through scattering media, which we are going to introduce in the following section. However, decorrelation will disrupt the focus by changing the transmission matrix [66]. The general solution is to speed up the system and keep its response time shorter than the decorrelation time, which we will discuss detailedly in Chapter 3.

1.4 Methods for Optical Focusing and Imaging through Scattering Media

In this section, we will give a brief review on the techniques to realize optical focusing and imaging through scattering media. The discussion will focus on the concepts and principles. First, we will talk about wavefront shaping, a novel method that enables optical focusing through scattering media. Then, we will go through different methods people use to realize imaging through scattering media. Finally, we will introduce techniques for glare suppression.

Wavefront shaping

Although focusing through scattering media has long been considered impossible, recent developments in wavefront shaping (WFS) have changed this view. The basic principle behind WFS is rooted in the transmission matrix theory. Let's first take a back look on Eq. 1.2.14:

$$\begin{bmatrix} e_{out,1} \\ e_{out,2} \\ \vdots \\ e_{out,N} \end{bmatrix} = \left[\begin{bmatrix} t_{11} \\ t_{21} \\ \vdots \\ t_{N1} \end{bmatrix} e_{in,1} + \begin{bmatrix} t_{12} \\ t_{22} \\ \vdots \\ t_{N2} \end{bmatrix} e_{in,2} + \cdots + \begin{bmatrix} t_{1M} \\ t_{2M} \\ \vdots \\ t_{NM} \end{bmatrix} e_{in,M} \right].$$

For a single output mode $e_{out,1}$, we have

$$e_{out,1} = t_{11}e_{in,1} + t_{12}e_{in,2} + \cdots + t_{1M}e_{in,M} = \sum_{k=1}^{N} t_{1k}e_{in,k}. \tag{1.4.1}$$

When the input is a plane wave, $e_{in,k}$ is identical for $k \in [1, M]$. $t_{1k}e_{in,k}$ is out of phase for different k, resulting in $e_{out,1}$ as a speckle. If we can control the phase of $e_{in,k}$ and set $\arg(e_{in,k}) = -\arg(t_{1k})$, we can line $t_{1k}e_{in,k}$s up in the complex plane, as shown in Fig. 1.9(b). Let $e'_{out,1}$ be the output after we optimize the phase of each input mode, then $|e'_{out,1}|$can be expressed as

$$|e'_{out,1}| = \sum_{k=1}^{N} \left| |t_{1k}| e^{\arg(t_{1k})} |e_{in,k}| e^{\arg(e_{in,k})} \right| = \sum_{k=1}^{M} |t_{1k}||e_{in,k}|. \tag{1.4.2}$$

Comparing to its modulus before the optimization, $|e_{out,1}|$, which is

$$|e_{out,1}| = |\sum_{k=1}^{M} t_{1k}e_{in,k}|, \tag{1.4.3}$$

we can derive the intensity enhancement factor η as

$$\eta = \frac{<|e'_{out,1}|^2>}{<|e_{out,1}|^2>} = \frac{\left\langle \left| \sum_{k=1}^{M} |t_{1k}||e_{in,k}| \right|^2 \right\rangle}{\left\langle | \sum_{k=1}^{M} t_{1k} e_{in,k}|^2 \right\rangle} = \frac{\left\langle \left| \sum_{k=1}^{M} |t_{1k}| \right|^2 \right\rangle}{\left\langle | \sum_{k=1}^{M} t_{1k}|^2 \right\rangle}. \tag{1.4.4}$$

Then we try to figure out the intensity of unoptimized modes (the background), it can be proved that their mean intensity before and after optimization are nearly the same, when M is much greater than N [35, 40]. $<|e_{out,1}|^2>$ is equal to the background before optimization, so $<|e_{out,1}|^2>$ can approximate the background after optimization as well. Therefore, η is also the signal to background ratio or peak to background ratio (PBR) after WFS. From the statistics of a transmission matrix,

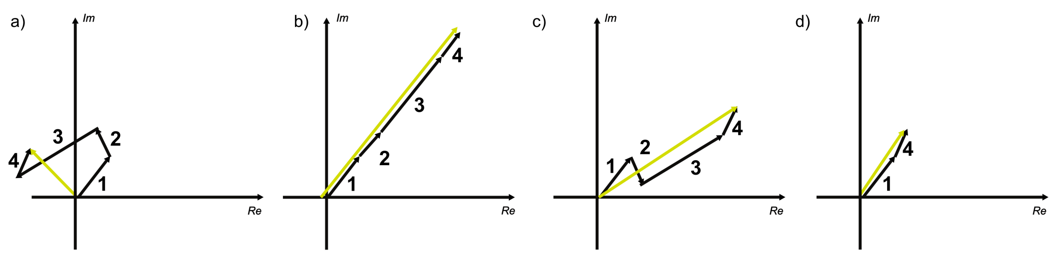

Figure 1.9: Schematic depiction of different modulation strategies. (a) Original unmodulated phasors out of phase. (b) Phase modulation. (c) Binary phase modulation. (d) Binary amplitude modulation.

we know that t_{1k} follows circular Gaussian distribution, then we can find $\eta = \frac{\pi}{4}M$. If we want to enhance the intensity in multiple output modes, going through the same calculation, we find that $\eta = \frac{\pi}{4}\frac{M}{N}$, where N is the number output modes to optimize. If we "shape" the input wavefront, we can focus light to a small region through scattering media.

The modulation of input modes can be relaxed to binary phase modulation or binary amplitude modulation in different experimental scenarios, which will still lead to an enhancement in the target output modes as shown in Fig.1.9(c) and (d). Fig.1.9(c) depicts the method by which binary phase modulation enhances the target output mode. If we shift the phase of phasor 2 and 3 by π, then all the output modes are partially lined up. In contrast, for binary amplitude modulation, we switch off all the input modes that negatively contribute to the the target output mode intensity. As shown in in Fig. 1.9(d), we turned off phasor 2 and 3 and only used phasor 1 and 4. Going through the same calculation of enhancement factor as in Eq. 1.4.4, we can summarize η for different modulation strategies as follows:

$$\begin{aligned}\eta_{phase\ modulation} &= \frac{\pi}{4}\frac{M}{N},\\ \eta_{binary\ phase} &= \frac{1}{\pi}\frac{M}{N},\\ \eta_{binary\ amplitude} &= \frac{1}{2\pi}\frac{M}{N},\end{aligned} \tag{1.4.5}$$

where M is the number of controllable input modes, and N is the number of output modes to optimize. Chapter 3 is an example of application of binary amplitude modulation, a more detailed discussion on this strategy can be found in the principle section.

Thanks to the development of modern electronics technology, a spatial light modulator (SLM) can be used to shape the wavefront in practice. An SLM could be either a LCOS-SLM (liquid crystal on silicon-Spatial Light Modulator), a ferroelectric LC-SLM (liquid crystal-spatial light modulator) or a DMD (digital micromirror device), which can realize phase modulation, binary phase modulation or binary amplitude modulation, respectively. Then the question comes to how to find out the correct input wavefront. In general, the correct wavefront can be obtained by iterative optimization [72–80], measuring the transmission matrix [81–85] or by phase conjugation [86–95]. Iterative optimization requires a feedback signal that quantifies how much intensity is focused on the target modes. The feedback signal can be fluorescent light from a probe particle [72–74], photoacoustic wave [75, 76], ultrasound [77], second-harmonic generation [78], two-photon or multi-photon excitation [79, 80] or light intensity in the corresponding modes measured by a photodetector [40]. Iterative methods inherently suffers from a relatively long time of convergence, since the solution is found through trial and error. Transmission matrix measurement [81–85] can be deemed as an extension of iteration optimization. It is equivalent to figuring out the optimum input wavefront to all the output modes of interest. Transmission matrix measurement figures out the transmission matrix by measuring the output wavefronts with the pre-knowledge of corresponding input wavefronts. We can expect that transmission matrix measurement is even more time-consuming than iterative optimization. Moreover, in most situations of application, it requires direct access to the output plane.

Phase conjugation will be detailedly discussed in chapter 2 and 3. Here, we just give a brief introduction to the principle. Phase conjugation describes the reciprocity of light propagation in a linear and lossless medium [96, 97]: the phase conjugate

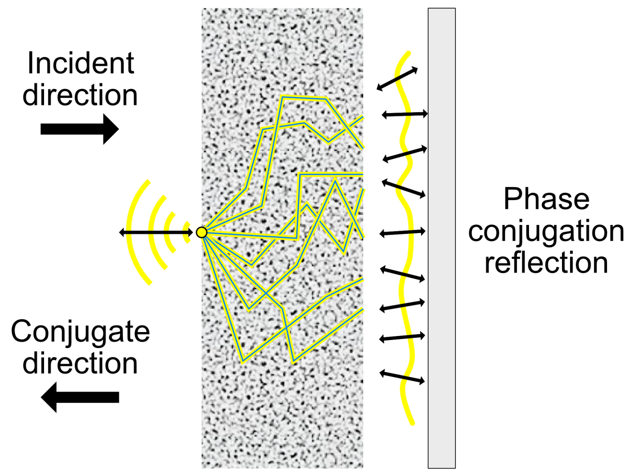

Figure 1.10: Schematic depiction of phase conjugation

reflection of a wavefront is a "time-reversed" replica of the wavefront's electric field. As shown in Fig.1.10, if we place a point source at the target mode, then light will propagate through the scattering medium and generate an output wavefront. At the output plane, if the wavefront is reflected off the output plane with a conjugate phase, scattered light will retrace their propagation and result in light focusing back at the target mode, as if time is reversed. From the process of phase conjugation, we know that, if we can have a focus at the target mode, the correct input wavefront for WFS can be easily figured out by measuring the wavefront coming out of the scattering media and conjugating the measured phase. However, the requirement to originally have a focus at the target mode where we aim to focus defeats the purpose of WFS. A way around this problem is to phase conjugate light from a guide star [98]. A guide star could be a small fluorescent particle [88] or a second harmonic generating particle [86] embedded in the scattering media. An alternative approach is to use ultrasound tagging to create a virtual guide star [67, 87, 89]. However, these guide stars all have their limits and disadvantages in application. For example, it is difficult to place small particles to a designated position without direct access to the target plane. For ultrasound tagging, the tagged photons are only a small portion compared to the total number of photons sent in, which may lead to a small signal to background ratio in the captured wavefront. Therefore, more noninvasive guide stars with better control and higher efficiency are still waiting to be discovered.

Methods for imaging through scattering media

Generally speaking, three approaches can be used to realize imaging through scattering media in the diffusive regime. The first is to scan the focus obtained by WFS. From the discussion in the previous section, we know a tight focus can be formed through scattering media by WFS. If the WFS technique used, like TRUE technique [67, 87], has ability to select an arbitrary mode through the scattering media, then we are able to scan the focus over the object. Scanning can also be realized with the assistant of memory effect [99], but it has limitation in the thickness of the scattering media and scanning range. Moreover, the object has to be placed at a distance behind the scattering media. Focus scanning approaches also require the signal generated by the object to be distinguished by the detector from the input light. Therefore, existing demonstration is limited to a fluorescent [67] or second harmonic generating [99] object.

The second approach is measuring the transmission matrix [81, 100]. As aforementioned in the transmission matrix section, transmission matrix describes the transform between input wavefront and output wavefront. In an imaging scenario, the input wavefront is the optical field to be found from the object, while output wavefront can be obtained from measurement. If we know the transmission matrix, then the object can be figured out by solving the inverse problem of the transform. As discussed in the WFS section, it is difficult to acquire the pre-knowledge of transmission matrix without access to the object plane. This approach shares the same limit with transmission matrix measurement in WFS. The third approach is the speckle-correlation-based imaging (SCI) [79, 101, 102], which we will discuss in detail in chapter 5. In general, optical imaging through scattering media still has a long way to go for application.

Methods for glare suppression

The optical field associated with glare and the reflected optical field from a remote target is different in an important way. Specifically, the glare components generally have a shorter optical path from source to detector. In principle, glare suppression can be performed using time-of-flight (TOF) methods [103–106] with the help of fast imaging systems, such as intensified charge-coupled device (ICCD) [107]. A TOF method would discard glare photons by binning the arriving light based on arrival time. Unfortunately, the requisite devices are very costly and, worse, tend to have very finite operating lifetime. There are some interesting developments in the use of modulated illumination and post-detection processing to achieve TOF gating electronically [108]. One limitation for these methods is that they need to contend with glare associated noise, as the glare is not suppression prior to detection. Methods such as light detection and ranging (LIDAR) [109] can detect targets occluded by glare by coherently gated (CG) detection of light that have travelled a specific path length (or path length range). CG methods have a target range limitation—targets beyond the coherence length of the light source cannot be detected [110]. You will find more discussions on various glare suppression techniques in chapter 5. In general, there is not a comprehensive solution for glare suppression, as you can feel on the road when driving in a foggy day.

1.5 Outline of This Thesis

In this thesis, we will explore solutions to the problem of scattering from different aspects. Chapter 2 and 3 will aim on optical focusing through scattering media, while chapter 4 and 5 aim on imaging. Chapter 2 talks about Time Reversal by Analysis of Changing wavefronts from Kinetic targets (TRACK) technique. We will show that the motion of object can be incorporated as a guide star in phase conjugation. We will demonstrate that by taking the difference between time-varying scattering fields caused by a moving object and applying optical phase conjugation, light can be focused back to the location previously occupied by the object. Chapter 3 tackles the decorrelation problem in wavefront shaping. We will talk about our strategies to speed up a DOPC system and demonstrate that our system is fast enough to focus light through 2.3mm-thick living mouse skin, which has a potential to transfer wavefront shaping to *in vivo* applications. Chapter 4 introduces a glare suppression method based on destructive interference. We will show an optical analogue to noise canceling headphones and some experimental results in imaging through strongly backscattering media. Finally, in chapter 5, we will demonstrate a method to image a moving target through scattering media noninvasively. Its principle roots are in the speckle-correlation-based imaging (SCI) invented by Ori Katz. We will talk about how we improved the technique and extended its application to a bright field imaging scenario.

References

[1] Max Born and Emil Wolf. *Principles of optics: electromagnetic theory of propagation, interference and diffraction of light*. Elsevier, 1980.

[2] BJ Lin. *Optical methods for fine line lithography*. Elsevier, North Holland, 1980.

[3] Marc D Levenson, NS Viswanathan, and Robert A Simpson. “Improving resolution in photolithography with a phase-shifting mask”. In: *IEEE Transactions on electron devices* 29.12 (1982), pp. 1828–1836.

[4] Thomas J Dougherty et al. “Photodynamic therapy”. In: *Journal of the National Cancer Institute* 90.12 (1998), pp. 889–905.

[5] Graham CR Ellis-Davies. “Caged compounds: photorelease technology for control of cellular chemistry and physiology”. In: *Nature methods* 4.8 (2007), pp. 619–628.

[6] Karl Deisseroth. “Optogenetics”. In: *Nature methods* 8.1 (2011), pp. 26–29.

[7] Ofer Yizhar et al. “Optogenetics in neural systems”. In: *Neuron* 71.1 (2011), pp. 9–34.

[8] Sylvie Hénon et al. “A new determination of the shear modulus of the human erythrocyte membrane using optical tweezers”. In: *Biophysical journal* 76.2 (1999), pp. 1145–1151.

[9] JP Mills et al. “Nonlinear elastic and viscoelastic deformation of the human red blood cell with optical tweezers”. In: *MCB-TECH SCIENCE PRESS-* 1 (2004), pp. 169–180.

[10] Mark C Pierce, David J Javier, and Rebecca Richards-Kortum. “Optical contrast agents and imaging systems for detection and diagnosis of cancer”. In: *International journal of cancer* 123.9 (2008), pp. 1979–1990.

[11] Jerome Mertz. *Introduction to optical microscopy*. Vol. 138. CSIRO, 2010.

[12] Stefan W Hell and Jan Wichmann. “Breaking the diffraction resolution limit by stimulated emission: stimulated-emission-depletion fluorescence microscopy”. In: *Optics letters* 19.11 (1994), pp. 780–782.

[13] Mats GL Gustafsson. “Nonlinear structured-illumination microscopy: wide-field fluorescence imaging with theoretically unlimited resolution”. In: *Proceedings of the National Academy of Sciences of the United States of America* 102.37 (2005), pp. 13081–13086.

[14] Michael J Rust, Mark Bates, and Xiaowei Zhuang. “Sub-diffraction-limit imaging by stochastic optical reconstruction microscopy (STORM)”. In: *Nature methods* 3.10 (2006), pp. 793–796.

[15] Eric Betzig et al. “Imaging intracellular fluorescent proteins at nanometer resolution”. In: *Science* 313.5793 (2006), pp. 1642–1645.

[16] Dong Li et al. "Extended-resolution structured illumination imaging of endocytic and cytoskeletal dynamics". In: *Science* 349.6251 (2015), aab3500.

[17] Joseph Goldstein et al. *Scanning electron microscopy and X-ray microanalysis: a text for biologists, materials scientists, and geologists*. Springer Science & Business Media, 2012.

[18] Yasushi Inouye and Satoshi Kawata. "Near-field scanning optical microscope with a metallic probe tip". In: *Optics letters* 19.3 (1994), pp. 159–161.

[19] Bert Hecht et al. "Scanning near-field optical microscopy with aperture probes: Fundamentals and applications". In: *The Journal of Chemical Physics* 112.18 (2000), pp. 7761–7774.

[20] E Hecht. "Optics 4th edition by Eugene Hecht Reading". In: *MA: Addison-Wesley Publishing Company* 1 (2001), p. 2001.

[21] Derek Albert Long and DA Long. *Raman spectroscopy*. McGraw-Hill New York, 1977.

[22] Mildred S Dresselhaus et al. "Raman spectroscopy of carbon nanotubes". In: *Physics reports* 409.2 (2005), pp. 47–99.

[23] LM Malard et al. "Raman spectroscopy in graphene". In: *Physics Reports* 473.5 (2009), pp. 51–87.

[24] Norman Colthup. *Introduction to infrared and Raman spectroscopy*. Elsevier, 2012.

[25] Andrew Weiner. *Ultrafast optics*. Vol. 72. John Wiley & Sons, 2011.

[26] Graham Fleming. "Chemical applications of ultrafast spectroscopy". In: (1986).

[27] Jagdeep Shah. *Ultrafast spectroscopy of semiconductors and semiconductor nanostructures*. Vol. 115. Springer Science & Business Media, 2013.

[28] Liang Gao et al. "Single-shot compressed ultrafast photography at one hundred billion frames per second". In: *Nature* 516.7529 (2014), pp. 74–77.

[29] *Mie Scattering and Rayleigh Scattering*. `http://hyperphysics.phy-astr.gsu.edu/hbase/atmos/blusky.html`. Accessed: 2017-04-10.

[30] Hendrik Christoffel Van de Hulst and V Twersky. "Light scattering by small particles". In: *Physics Today* 10.12 (1957), pp. 28–30.

[31] Craig F Bohren and Donald R Huffman. *Absorption and scattering of light by small particles*. John Wiley & Sons, 2008.

[32] Lihong V Wang and Hsin-i Wu. *Biomedical optics: principles and imaging*. John Wiley & Sons, 2012.

[33] *Mie Scattering Calculator*. `http://omlc.org/calc/mie_calc.html`. Accessed: 2017-04-10.

[34] Vasilis Ntziachristos. “Going deeper than microscopy: the optical imaging frontier in biology”. In: *Nature methods* 7.8 (2010), pp. 603–614.

[35] Ying Min Wang. “Deep tissue fluorescence imaging with time-reversed light”. PhD thesis. California Institute of Technology, 2013.

[36] Steven L Jacques. “Optical properties of biological tissues: a review”. In: *Physics in medicine and biology* 58.11 (2013), R37.

[37] Joseph W Goodman. *Speckle phenomena in optics: theory and applications*. Roberts and Company Publishers, 2007.

[38] Benjamin Judkewitz et al. “Translation correlations in anisotropically scattering media”. In: *Nature physics* 11.8 (2015), pp. 684–689.

[39] Carlo WJ Beenakker. “Random-matrix theory of quantum transport”. In: *Reviews of modern physics* 69.3 (1997), p. 731.

[40] Ivo Micha Vellekoop. “Controlling the propagation of light in disordered scattering media”. In: *arXiv preprint arXiv:0807.1087* (2008).

[41] Dietrich Marcuse. “Light transmission optics”. In: (1972).

[42] Shechao Feng et al. “Correlations and fluctuations of coherent wave transmission through disordered media”. In: *Physical review letters* 61.7 (1988), p. 834.

[43] Isaac Freund, Michael Rosenbluh, and Shechao Feng. “Memory effects in propagation of optical waves through disordered media”. In: *Physical review letters* 61.20 (1988), p. 2328.

[44] Itai Dror, Arnon Sandrov, and Norman S Kopeika. “Experimental investigation of the influence of the relative position of the scattering layer on image quality: the shower curtain effect”. In: *Applied optics* 37.27 (1998), pp. 6495–6499.

[45] Eitan Edrei and Giuliano Scarcelli. “Optical imaging through dynamic turbid media using the Fourier-domain shower-curtain effect”. In: *Optica* 3.1 (2016), pp. 71–74.

[46] Gregoire Tremblay, Robert Bernier, and Gilles Roy. “The shower curtain effect paradoxes”. In: *SPIE Remote Sensing*. International Society for Optics and Photonics. 2015, pp. 964107–964107.

[47] Diederik S Wiersma et al. “Localization of light in a disordered medium”. In: *Nature* 390.6661 (1997), pp. 671–673.

[48] Tal Schwartz et al. “Transport and Anderson localization in disordered two-dimensional photonic lattices”. In: *Nature* 446.7131 (2007), pp. 52–55.

[49] Mordechai Segev, Yaron Silberberg, and Demetrios N Christodoulides. "Anderson localization of light". In: *Nature Photonics* 7.3 (2013), pp. 197–204.

[50] Virendra N Mahajan. "Zernike circle polynomials and optical aberrations of systems with circular pupils". In: *Applied optics* 33.34 (1994), pp. 8121–8124.

[51] James C Wyant and Katherine Creath. "Basic wavefront aberration theory for optical metrology". In: *Applied optics and optical engineering* 11.s 29 (1992), p. 2.

[52] Robert Edward Fischer et al. *Optical system design*. Citeseer, 2000.

[53] Kurt Rossmann. "Point spread-function, line spread-function, and modulation transfer function: Tools for the study of imaging systems 1". In: *Radiology* 93.2 (1969), pp. 257–272.

[54] Glenn D Boreman. *Modulation transfer function in optical and electro-optical systems*. Vol. 21. SPIE press Bellingham, WA, 2001.

[55] Maths Abrahamsson and J Sjöstrand. "Impairment of contrast sensitivity function (CSF) as a measure of disability glare." In: *Investigative ophthalmology & visual science* 27.7 (1986), pp. 1131–1136.

[56] Aldo Badano and Michael J Flynn. "Image degradation by glare in radiologic display devices". In: *Medical Imaging 1997*. International Society for Optics and Photonics. 1997, pp. 222–231.

[57] David B Rensch and RK Long. "Comparative studies of extinction and backscattering by aerosols, fog, and rain at 10.6 μ and 0.63 μ". In: *Applied Optics* 9.7 (1970), pp. 1563–1573.

[58] Ronald TH Collis et al. *Visibility Measurement for Aircraft Landing Operations.* Tech. rep. DTIC Document, 1970.

[59] BJ Brinkworth. "Calculation of attenuation and back-scattering in cloud and fog". In: *Atmospheric Environment (1967)* 5.8 (1971), pp. 605–611.

[60] TEW Schumann. "Theoretical aspects of the size distribution of fog particles". In: *Quarterly Journal of the Royal Meteorological Society* 66.285 (1940), pp. 195–208.

[61] Barry H Friemel et al. "Speckle decorrelation due to two-dimensional flow gradients". In: *IEEE transactions on ultrasonics, ferroelectrics, and frequency control* 45.2 (1998), pp. 317–327.

[62] J David Briers, Glenn Richards, and Xiao Wei He. "Capillary blood flow monitoring using laser speckle contrast analysis (LASCA)". In: *Journal of biomedical optics* 4.1 (1999), pp. 164–175.

[63] Sabine Przibilla et al. “Sensing dynamic cytoplasm refractive index changes of adherent cells with quantitative phase microscopy using incorporated microspheres as optical probes”. In: *Journal of biomedical optics* 17.9 (2012), pp. 0970011–0970019.

[64] DJ Pine et al. “Diffusing wave spectroscopy”. In: *Physical review letters* 60.12 (1988), p. 1134.

[65] Virgile Viasnoff, Francois Lequeux, and DJ Pine. “Multispeckle diffusing-wave spectroscopy: A tool to study slow relaxation and time-dependent dynamics”. In: *Review of scientific instruments* 73.6 (2002), pp. 2336–2344.

[66] Mooseok Jang et al. “Relation between speckle decorrelation and optical phase conjugation (OPC)-based turbidity suppression through dynamic scattering media: a study on in vivo mouse skin”. In: *Biomedical optics express* 6.1 (2015), pp. 72–85.

[67] Ying Min Wang et al. “Deep-tissue focal fluorescence imaging with digitally time-reversed ultrasound-encoded light”. In: *Nature communications* 3 (2012), p. 928.

[68] Yan Liu et al. “Optical focusing deep inside dynamic scattering media with near-infrared time-reversed ultrasonically encoded (TRUE) light”. In: *Nature Communications* 6 (2015).

[69] Daifa Wang et al. “Focusing through dynamic tissue with millisecond digital optical phase conjugation”. In: *Optica* 2.8 (2015), pp. 728–735.

[70] Joshua Brake, Mooseok Jang, and Changhuei Yang. “Analyzing the relationship between decorrelation time and tissue thickness in acute rat brain slices using multispeckle diffusing wave spectroscopy”. In: *JOSA A* 33.2 (2016), pp. 270–275.

[71] Yan Liu et al. “Focusing light inside dynamic scattering media with millisecond digital optical phase conjugation”. In: *Optica* 4.2 (2017), pp. 280–288.

[72] IM Vellekoop et al. “Demixing light paths inside disordered metamaterials”. In: *Optics express* 16.1 (2008), pp. 67–80.

[73] Ivo M Vellekoop and Christof M Aegerter. “Scattered light fluorescence microscopy: imaging through turbid layers”. In: *Optics letters* 35.8 (2010), pp. 1245–1247.

[74] Elbert G van Putten, A Lagendijk, and AP Mosk. “Optimal concentration of light in turbid materials”. In: *JOSA B* 28.5 (2011), pp. 1200–1203.

[75] Fanting Kong et al. “Photoacoustic-guided convergence of light through optically diffusive media”. In: *Optics letters* 36.11 (2011), pp. 2053–2055.

[76] Antonio M Caravaca-Aguirre et al. “High contrast three-dimensional photoacoustic imaging through scattering media by localized optical fluence enhancement”. In: *Optics express* 21.22 (2013), pp. 26671–26676.

[77] Jian Wei Tay et al. “Ultrasonically encoded wavefront shaping for focusing into random media”. In: *Scientific reports* 4 (2014), p. 3918.

[78] Jochen Aulbach et al. “Spatiotemporal focusing in opaque scattering media by wave front shaping with nonlinear feedback”. In: *Optics express* 20.28 (2012), pp. 29237–29251.

[79] Ori Katz et al. “Noninvasive nonlinear focusing and imaging through strongly scattering turbid layers”. In: *Optica* 1.3 (2014), pp. 170–174.

[80] Jianyong Tang, Ronald N Germain, and Meng Cui. “Superpenetration optical microscopy by iterative multiphoton adaptive compensation technique”. In: *Proceedings of the National Academy of Sciences* 109.22 (2012), pp. 8434–8439.

[81] SM Popoff et al. “Image transmission through an opaque material”. In: *arXiv preprint arXiv:1005.0532* (2010).

[82] Wonjun Choi et al. “Transmission eigenchannels in a disordered medium”. In: *Physical Review B* 83.13 (2011), p. 134207.

[83] Hyeonseung Yu et al. “Measuring large optical transmission matrices of disordered media”. In: *Physical review letters* 111.15 (2013), p. 153902.

[84] Thomas Chaigne et al. “Controlling light in scattering media non-invasively using the photoacoustic transmission matrix”. In: *Nature Photonics* 8.1 (2014), pp. 58–64.

[85] Angélique Drémeau et al. “Reference-less measurement of the transmission matrix of a highly scattering material using a DMD and phase retrieval techniques”. In: *Optics express* 23.9 (2015), pp. 11898–11911.

[86] Chia-Lung Hsieh et al. “Digital phase conjugation of second harmonic radiation emitted by nanoparticles in turbid media”. In: *Optics express* 18.12 (2010), pp. 12283–12290.

[87] Xiao Xu, Honglin Liu, and Lihong V Wang. “Time-reversed ultrasonically encoded optical focusing into scattering media”. In: *Nature photonics* 5.3 (2011), pp. 154–157.

[88] Ivo M Vellekoop, Meng Cui, and Changhuei Yang. “Digital optical phase conjugation of fluorescence in turbid tissue”. In: *Applied physics letters* 101.8 (2012), p. 081108.

[89] Ke Si, Reto Fiolka, and Meng Cui. “Fluorescence imaging beyond the ballistic regime by ultrasound-pulse-guided digital phase conjugation”. In: *Nature photonics* 6.10 (2012), pp. 657–661.

[90] Ke Si, Reto Fiolka, and Meng Cui. "Breaking the spatial resolution barrier via iterative sound-light interaction in deep tissue microscopy". In: *arXiv preprint arXiv:1208.5264* (2012).

[91] Benjamin Judkewitz et al. "Speckle-scale focusing in the diffusive regime with time reversal of variance-encoded light (TROVE)". In: *Nature photonics* 7.4 (2013), pp. 300–305.

[92] Cheng Ma et al. "Time-reversed adapted-perturbation (TRAP) optical focusing onto dynamic objects inside scattering media". In: *Nature photonics* 8.12 (2014), pp. 931–936.

[93] Edward Haojiang Zhou et al. "Focusing on moving targets through scattering samples". In: *Optica* 1.4 (2014), pp. 227–232.

[94] Haowen Ruan et al. "Iterative time-reversed ultrasonically encoded light focusing in backscattering mode". In: *Scientific reports* 4 (2014), p. 7156.

[95] Yuta Suzuki et al. "Continuous scanning of a time-reversed ultrasonically encoded optical focus by reflection-mode digital phase conjugation". In: *Optics letters* 39.12 (2014), pp. 3441–3444.

[96] Amnon Yariv. "Phase conjugate optics and real-time holography". In: *IEEE Journal of Quantum Electronics* 14.9 (1978), pp. 650–660.

[97] Peter Günter. "Holography, coherent light amplification and optical phase conjugation with photorefractive materials". In: *Physics Reports* 93.4 (1982), pp. 199–299.

[98] Roarke Horstmeyer, Haowen Ruan, and Changhuei Yang. "Guidestar-assisted wavefront-shaping methods for focusing light into biological tissue". In: *Nature photonics* 9.9 (2015), pp. 563–571.

[99] Chia-Lung Hsieh et al. "Imaging through turbid layers by scanning the phase conjugated second harmonic radiation from a nanoparticle". In: *Optics express* 18.20 (2010), pp. 20723–20731.

[100] Huichang Zhuang et al. "High speed color imaging through scattering media with a large field of view". In: *Scientific Reports* 6 (2016).

[101] Jacopo Bertolotti et al. "Non-invasive imaging through opaque scattering layers". In: *Nature* 491.7423 (2012), pp. 232–234.

[102] Amir Porat et al. "Widefield lensless imaging through a fiber bundle via speckle correlations". In: *Optics Express* 24.15 (2016), pp. 16835–16855.

[103] *Range-Gating Technology*. `http://www.obzerv.com/en/range-gating-technology/core-expertise/`. Accessed: 2017-04-10.

[104] Martin Laurenzis and Arnaud Woiselle. "Laser gated-viewing advanced range imaging methods using compressed sensing and coding of range-gates". In: *Optical Engineering* 53.5 (2014), pp. 053106–053106.

[105] David Monnin et al. “Active-imaging-based underwater navigation”. In: *SPIE Security+ Defence*. International Society for Optics and Photonics. 2015, 96490H–96490H.

[106] Frank Christnacher et al. “Influence of gating and of the gate shape on the penetration capacity of range-gated active imaging in scattering environments”. In: *Optics express* 23.26 (2015), pp. 32897–32908.

[107] M Teschke et al. “High-speed photographs of a dielectric barrier atmospheric pressure plasma jet”. In: *IEEE Transactions on Plasma Science* 33.2 (2005), pp. 310–311.

[108] Achuta Kadambi et al. “Frequency domain ToF: encoding object depth in modulation frequency”. In: *arXiv preprint arXiv:1503.01804* (2015).

[109] Claus Weitkamp. *Lidar: range-resolved optical remote sensing of the atmosphere*. Vol. 102. Springer Science & Business, 2006.

[110] David Huang et al. “Optical coherence tomography”. In: *Science (New York, NY)* 254.5035 (1991), p. 1178.